Event-based cameras: a comparative study for fluid event detection.

A. Court*, C. Bruecker

Dept. Engineering, City, University of London, UK

*Corresponding author: alecsandra.court.2@city.ac.uk

Keywords: Event-based camera, PIV processing, fluid flow.

ABSTRACT

A feasibility study using an event-based camera for the detection of plane-wise motion of a 2D array of bio-inspired sensing pillars to detect generated flow events. EBCs show potential for future applications where PIV may have been classically used. They have the benefit of only generating data when an event happens and with comparatively cheaper setups, they hold great potential for flow monitoring. EBCs collect pixel x and y locations, as well as pixel contrast change data at each time there is an event and can be trained on regions of interest. Comparative experiments were carried out in the labs at City, University of London, to investigate the feasibility of using EBCs for the detection of generated large flow structures in both air and water. The disturbances were produced by a gust generator, an upstream cylinder and an air gun for a variety of controlled situations, such as disturbances caused by gusts, crossflows and wake downstream oscillations. Some results were also compared to known PIV results from our lab to see how EBCs can detect a known flow structure over the sensing pillars. The results presented demonstrate the capability of the pillars and EBC to detect large flow structures. These initial results show promise for future applications of flow monitoring, such as real-time flow monitoring via a machine learning algorithm that is trained to detect certain flow patterns over the sensing pillars. This would be an intermediate step into a fully automated flow control loop.

1. Introduction

Classical frame-based cameras produce set-size images at set time intervals, providing large amounts of data regardless of whether something has changed in the field of view from the last time stamp. Event-based cameras, EBCs, capture data asynchronously in the form of a timestamp, pixel x and y locations and pixel contrast changes. This results in areas of view with no data, meaning that no pixel change has occurred and areas where change has occurred, either positive (bright) or negative (darker).

EBCs are not new technology, with the fundamental concepts having been discussed since the 90's in Mahowald (1992) and Mead (1989). More recently, there has been work published on computer

vision by Lichtsteiner et al. (2008) and Son et al. (2017). The interest in these cameras has grown in recent years due to their relatively low cost compared to other high-speed setups Delbruck & Lichtsteiner (2007). However, the output of these cameras are very different to standard frame-based cameras, thus requiring novel processing techniques, as discussed in Gallego et al. (2022).

Researchers are now looking at applying EBCs to areas such as fluid dynamics for the application of particle image velocimetry, PIV. C. E. Willert (2023) discusses the uses of EVBs for PIV and the shortcomings that they have, it is found that an EVB and a low-cost pulsed laser provide a cost-effective alternate method of PIV measurement. From the same lab, C. Willert & Klinner (2023), time-resolved PIV was successfully carried out with an EVB as opposed to a high-speed camera. The found result was that the described system was able to produce high-quality data, equivalent to expensive high-speed camera setups at 10kHz.

In our lab, at City, University of London, work has already been carried out on the development and testing of a pneumatic gust generator, Court et al. (2023) as well as bio-inspired silicone sensing hairs Court & Bruecker (2024). The silicone sensing pillars are an ideal candidate for EBCs, as they are set event areas with only single plane movement, reducing the post-processing filtering requirement.

The layout of the paper is such that; experimental methods are detailed after the introductory chapter, followed by the experimental setup. After this, the results of the initial experiments are presented in the form of snapshot images and overlays. Lastly, discussions and concluding remarks are drawn.

2. Background

The experiments utilised two models, a gust generator used to generate upstream disturbances and a sensing model used to detect flow structures. The two models have already been designed and tested in our lab, they are described in detail in Court et al. (2023). The below figure 1, shows the array of flexible sensing pillars integrated into an aerofoil, the tips of the pillars are marked with a fluorescent dye (MMA-RhB-Frak-Paticles, Dantec Dynamics) and viewed via a colour filter lens to ensure the tips are easily identifiable by the camera. The sensors are silicone and have a rectangular cross-section allowing for movement in the streamwise plane. The pneumatically actuated flaplet model will be referred to as the gust model and the bio-inspired flexible pillar model, the sensing model.

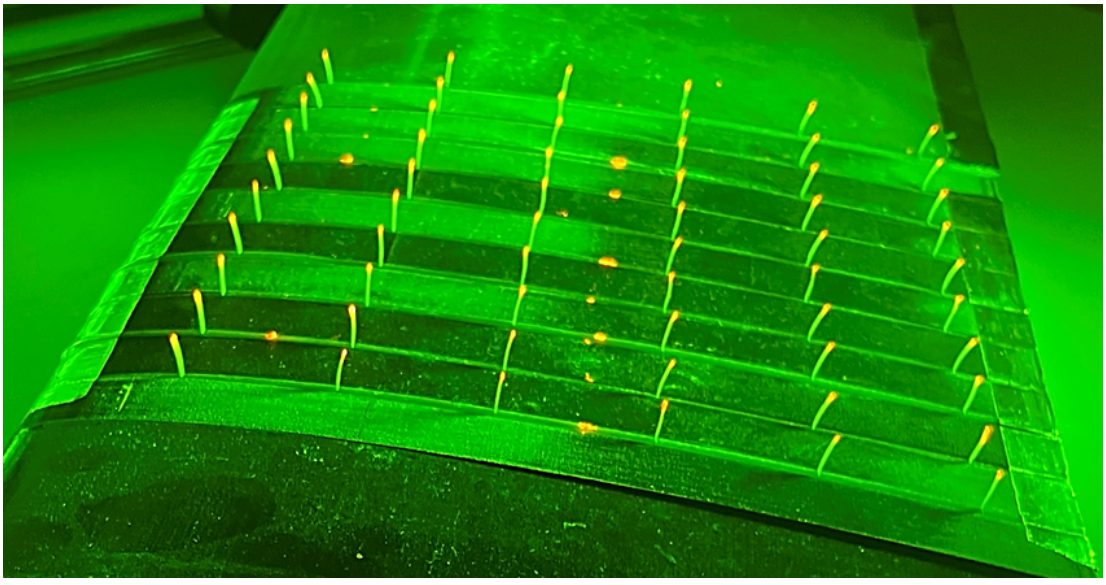

Figure 1. Photo of the sensing pillar array, with marked tips shown under green LED, taken from Court et al. (2023).

The EBC used in this paper was the EVK4 HD by PROPHESEE. Their camera was inspired by the functions of the human eye, where photoreceptors in the back of the eye turn the incoming light into signals, these signals are then processed in the brain via the optic nerve. Much like the photoreceptors, the pixels react independently and asynchronously to scene light changes. The result is sparse event data, driven only by changes in the scene.

Events generated by the event sensor are represented by two colours; light blue to show increased light intensity (positive contrast change, polarity=1, "ON") and dark blue to show decreased light intensity (negative contrast change, polarity=0, "OFF"), where there are no events the colour will be black or white depending on the chosen colour schemes. When a pixel detects an event, it is transmitted to the on-demand readout, along with the timestamp, x and y positions and polarity of the contrast change.

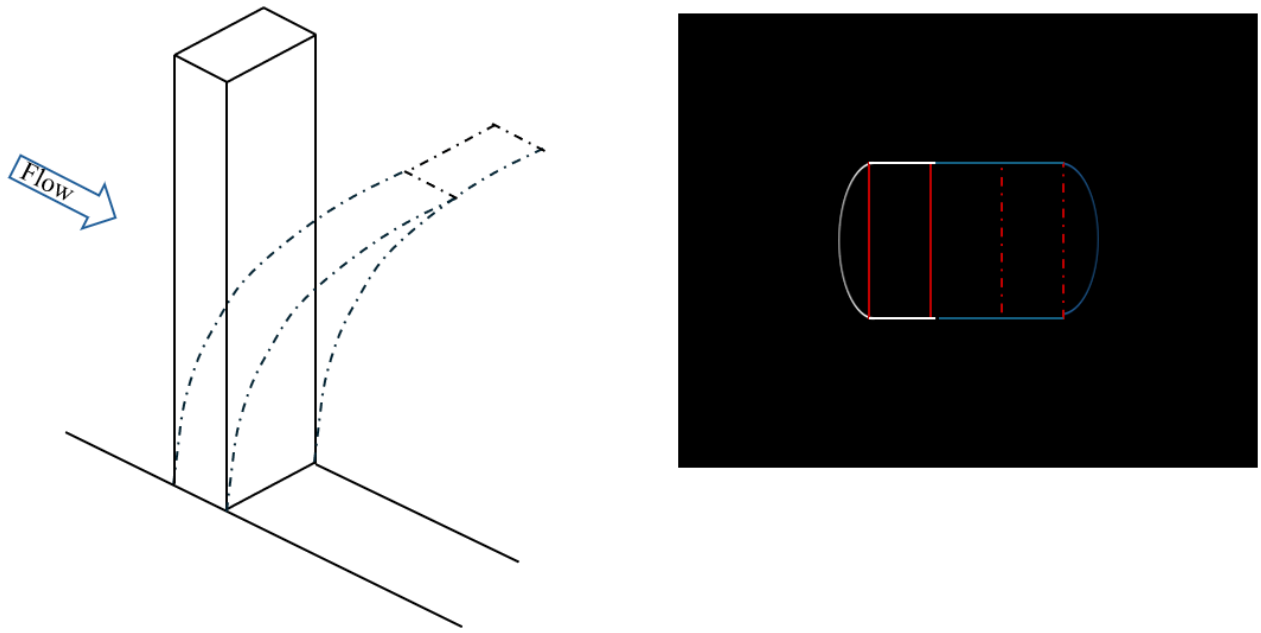

Figure 2. Schematic of the movement of the pillars as outputted by the camera.

The above figure, 2, shows the streamwise bending of the pillars due to oncoming flow on the left and the top-down view of the movement of the bending pillar on the right. The right-hand view is shown as how the camera shows the data, with the red boxes to show pillar movement overlaid. The white and blue lines represent a very simplified image that would be outputted, they represent the shape of the pixel spread detecting a change event.

3. Experimental Setup

Two measurement setups were used, a dynamic water test and a static air test to obtain a wider variety of results. The tunnel used was the water tunnel at City, University of London. The water setup for this paper follows largely the same structure as the setups described in Court & Bruecker (2024), for ease of comparison. The camera used for the measurements was an event-based camera (Prophesee EVK4 HD),1280 x 720 with a colour filter fitted. The filter was to aid in the visibility of the pillar tips, (marked with fluorescent dye), it was a green light filter (long-pass optical filter, cut-off wavelength of 550 nm, Edmund Optics). The cross-section of interest was illuminated by Dantec raypower 5000 5W continuous wave Argon-Ion laser (λ=532nm) with sheet thickness 1mm. The laser was mounted outside the tunnel and the beam reflected such that it illuminated the region of interest vertically from below.

3.1. Dynamic water test

3.1.1. With Gust Generator

Here, the gust generator model was set upstream of the sensing model by a third of a chord length and mounted vertically in the tunnel. The free ends of the models were against the lower viewing window and above the free surface, as to avoid wave formation. The models were placed offset of the centre of the tunnel so that the trailing edge of the gust model aligned in the same place as the sensing model's leading edge. The tunnel velocity used was 35cm/s.

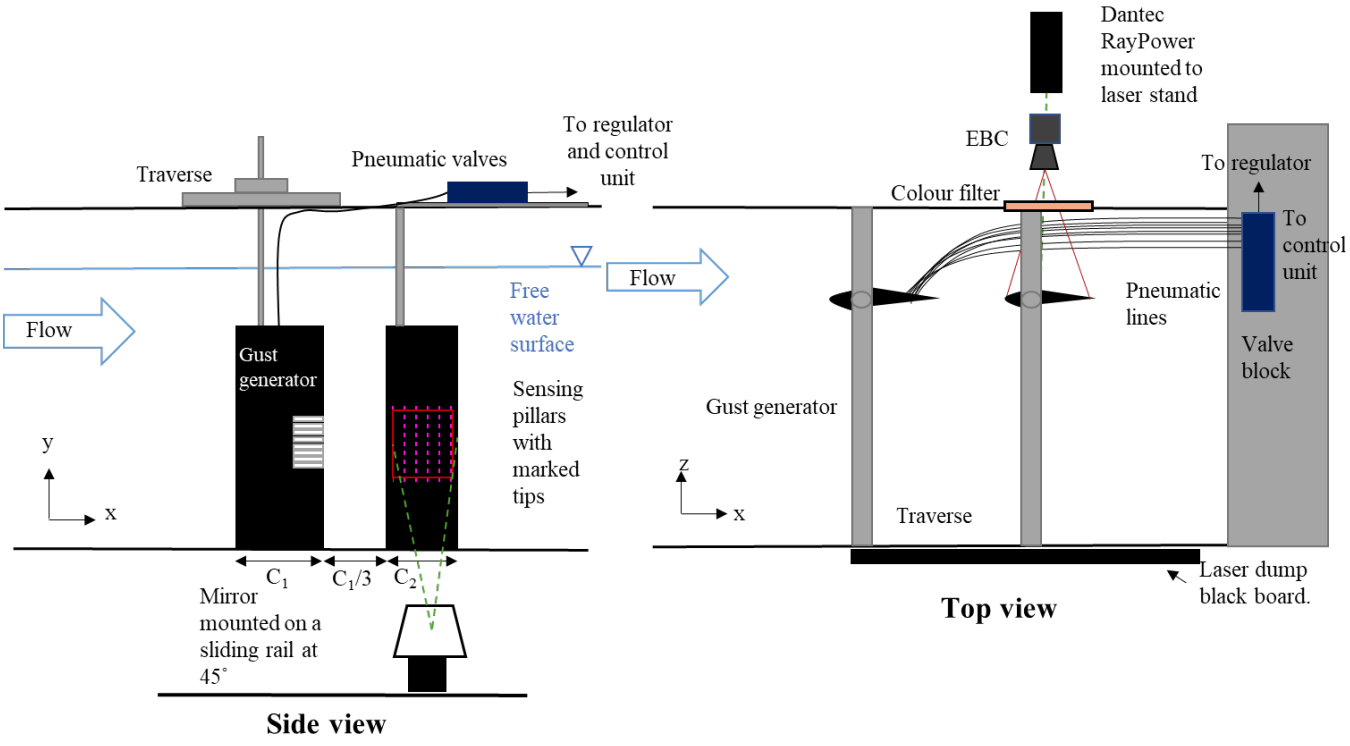

Figure 3. Schematic of the dynamic experimental setup in water with the gust generator.

The above figure, 3, shows the setup for the first of the dynamic water setups. C_1 corresponds to the chord length of the gust generate model, 30cm and C_2 the sensing model of 20cm.

The tunnel was run and allowed to settle to the chosen velocity, after which the gusts were generated via the opening and closing of the flaplets on the gust mode. This disturbance was recorded over the sensing pillars via the EBC.

3.1.2. With Upstream Cylinder

The next set of dynamic water tests were done without the upstream gust model and instead had a cylinder mounted upstream to produce constant shedding frequencies. The velocity of the tunnel was again, 35cm/s and the diameter of the cylinder was 2.7cm. The below figure, 4, shows the setup. the cylinder was mounted perpendicular to the leading edge of the sensing model, centred on the middle row of sensing pillars.

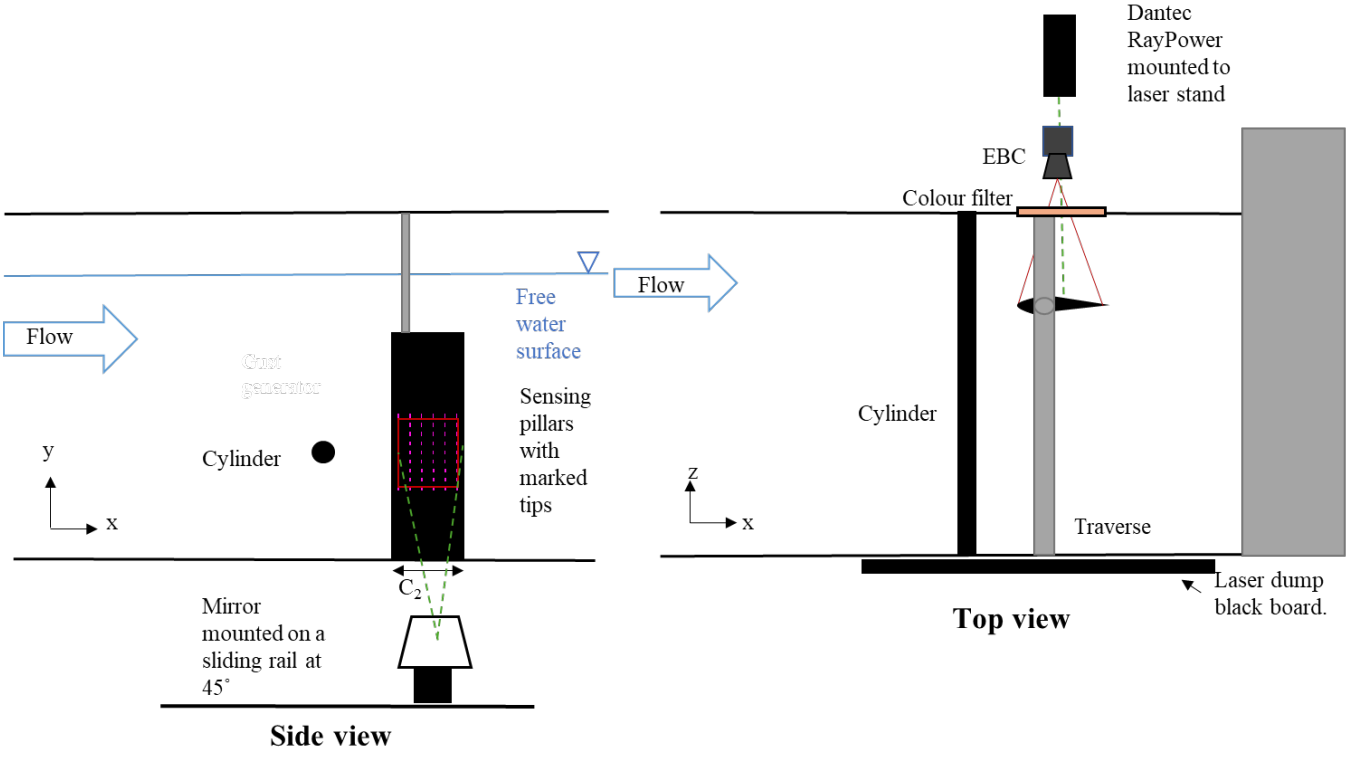

Figure 4. Schematic of the dynamic experimental setup in water with the upstream cylinder.

Like the gust recordings, the tunnel was set to the chosen velocity and allowed to settle. Recordings were then taken of the sensing pillars, as they were constantly disturbed by the upstream cylinder.

3.2. Static air test

The secondary set of measurements were taken statically in air, with the disturbance generated by a pneumatic air gun. The mounting of the sensing model, laser and camera was the same as described above, however, this test was done with a dry tunnel. The below figure, 5 shows the secondary setup.

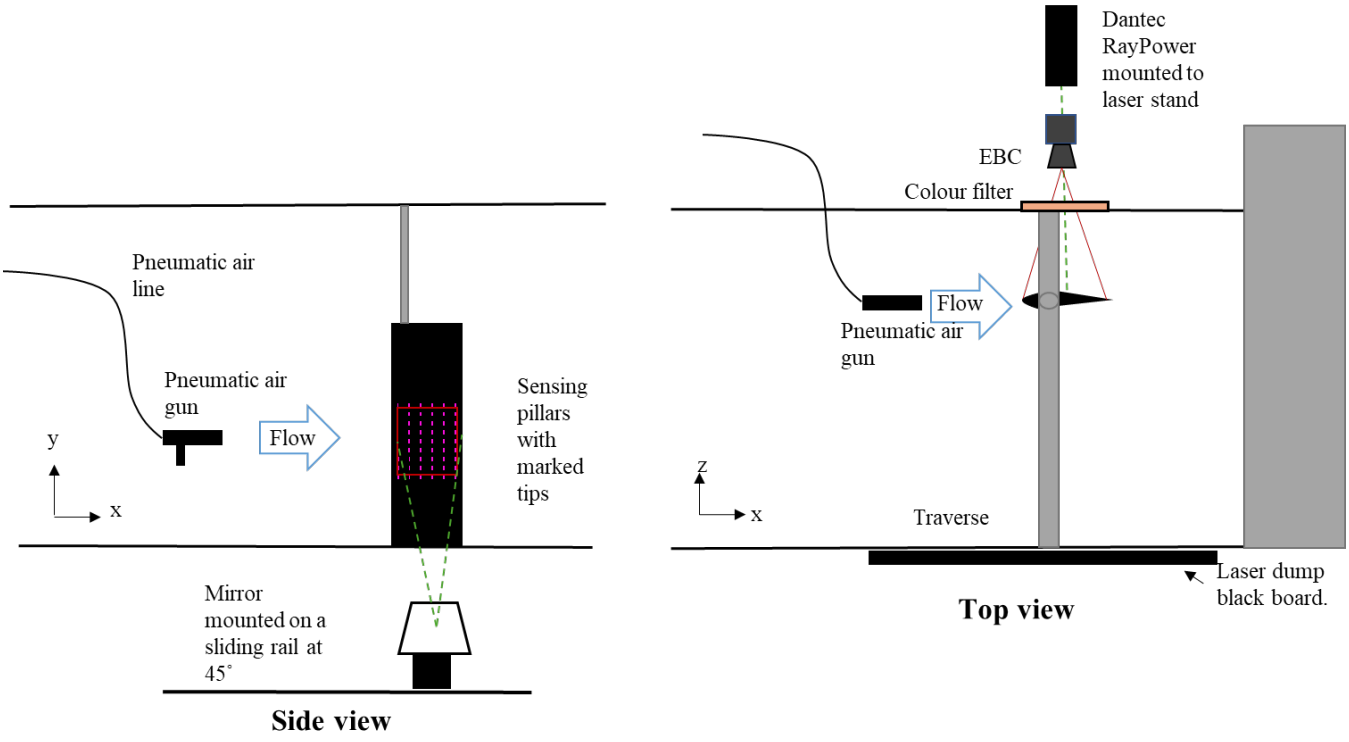

Figure 5. Schematic of the static experimental setup in air.

The air gun provided constant disturbance (held on), gusts (pulsed on and off in quick succession) and cross winds (the angle of the air gun changed relative to the central line of pillars). Recordings were taken of all situations.

4. Results

4.1. Dynamic water test

The dynamic water test experiments gave rise to an opportunity to look at both the disturbance from the generator and the inherent disturbance that arises from the wake of the upstream cylinder over the pillars.

4.1.1. With Gust Generator Upstream

Twenty stills from the EBC, corresponding to roughly 0.6s, in which the generated disturbance passed over the sensing pillars, were layered together to create the left-hand side of figure 6. The right-hand side of 6, is a quiver plot of the same flow structure of the pillars taken from Court & Bruecker (2024). It can be seen that the EBC can detect the same flow structure, we can see that

the central row of pillars are blue, indicating that the pillars are bending opposite to the freestream direction, which is seen on the quiver plot too. This region of flow retardation is bound by areas of flow acceleration, indicated by the white dots, showing the pillars bending in the same direction as the freestream velocity, this is also shown on the quiver plot.

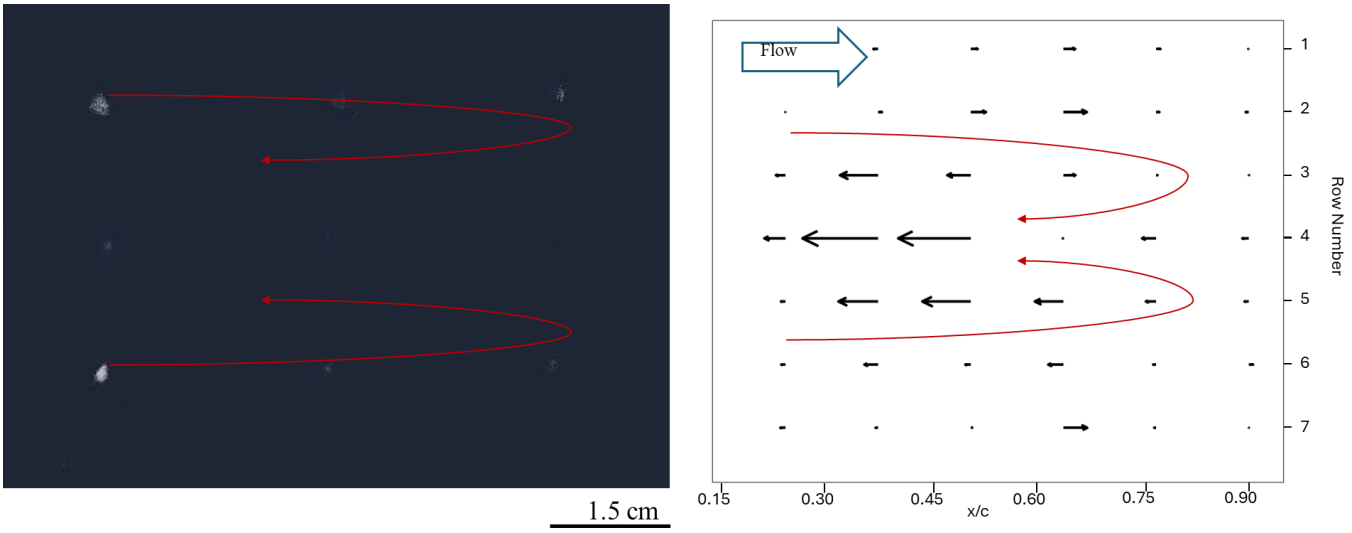

Figure 6. Comparison of layered EBC view and quiver plot from Court et al. (2023)

4.1.2. With Cylinder Upstream

The below figure, 7, is the probability density mapping of one pillar in the wake of the cylinder at 35cm/s freestream velocity. The figure shows a clear pattern of two bright areas, in which the pillar is at maximum velocity coming to inflection in forward and backward direction, relative to the mean. The figure was made by adding one pixel position over time, with a +1 in grey level each time an event happened at this position. Resulting in a grey level map from 0 to the total number of events. The maximum grey level is 225.

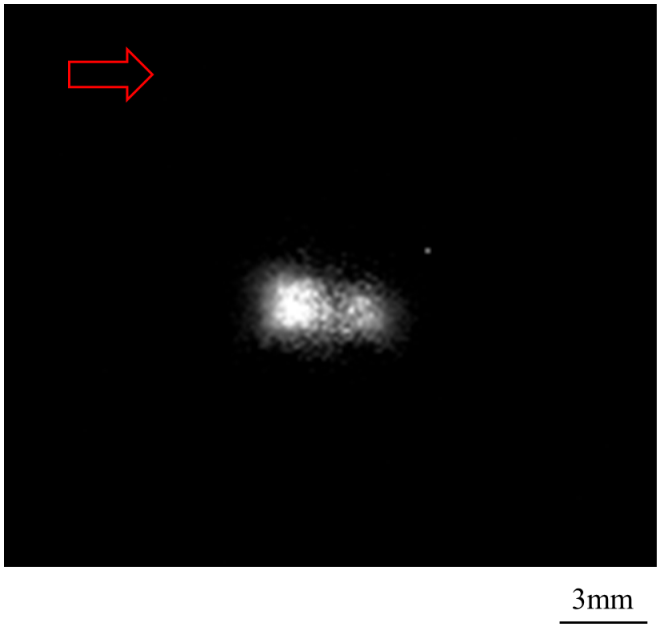

Figure 7. Enlarged view of one pillar probability density location, with red arrow to indicate flow direction.

The Reynold's number using the tunnel freestream velocity (35cm/s) and the diameter of the upstream cylinder (2.7cm) is $Re_{Cylinder} = 10^4$, using this and the below figure, 8, it can be seen that the expected Strouhal number, St, for the cylinder is around 0.2, assuming smooth surface.

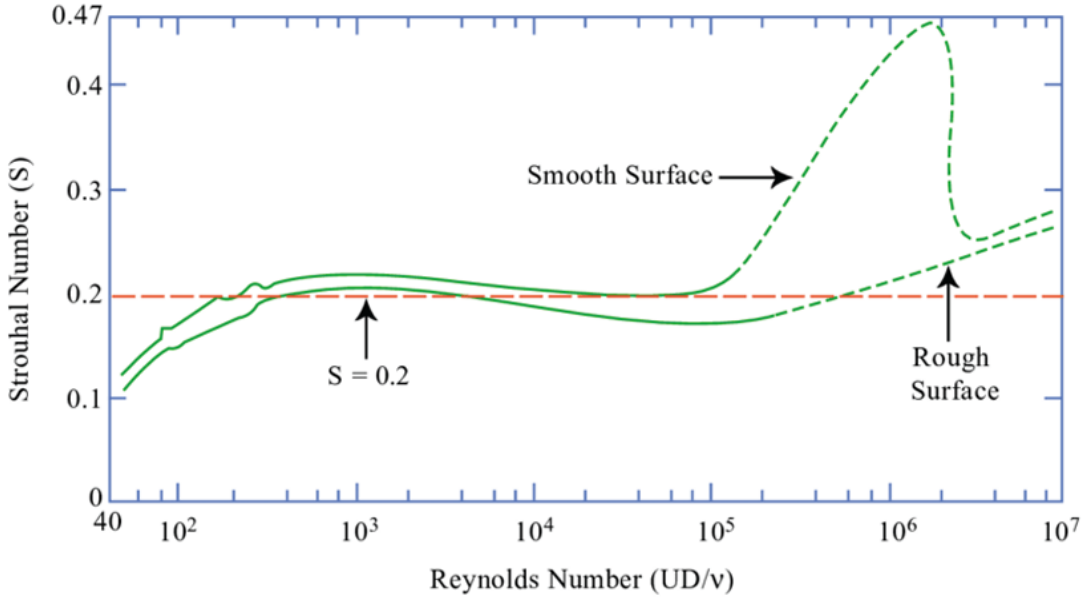

Figure 8. Graph showing the variation of Strouhal with Reynolds for a cylinder, as taken from Uruba & Procházka (2019)

Where St is defined below in 1, where f is the shedding frequency, D is the diameter of the obstructing cylinder and U is the freestream velocity.

$$St = fD/U \tag{1}$$

Using the recordings taken from the cylinder tests, it can be seen by eye that the pillars oscillate at a frequency of around 3 Hz. Two colour changes, ie white to blue, then blue to white were deemed one full oscillation of a pillar, corresponding to fully back, then fully forward. Substituting an f value of three into the above equation, 1, gives a St number of 0.23, showing that the pillars and EBC can pick up the oscillations from the upstream cylinders vortex trail.

4.2. Single gust disturbance

The disturbances generated by the pneumatic air gun as described in the experimental setup were categorised by snapshots of the outputted recordings. The below figure, 9, is two snapshots taken 0.2s apart during the gust testing phase. This was where the air gun was pulsed on and off in quick succession to generate gusts. This is a top-down view of the pillars in the vertical plane, as seen by the EBC.

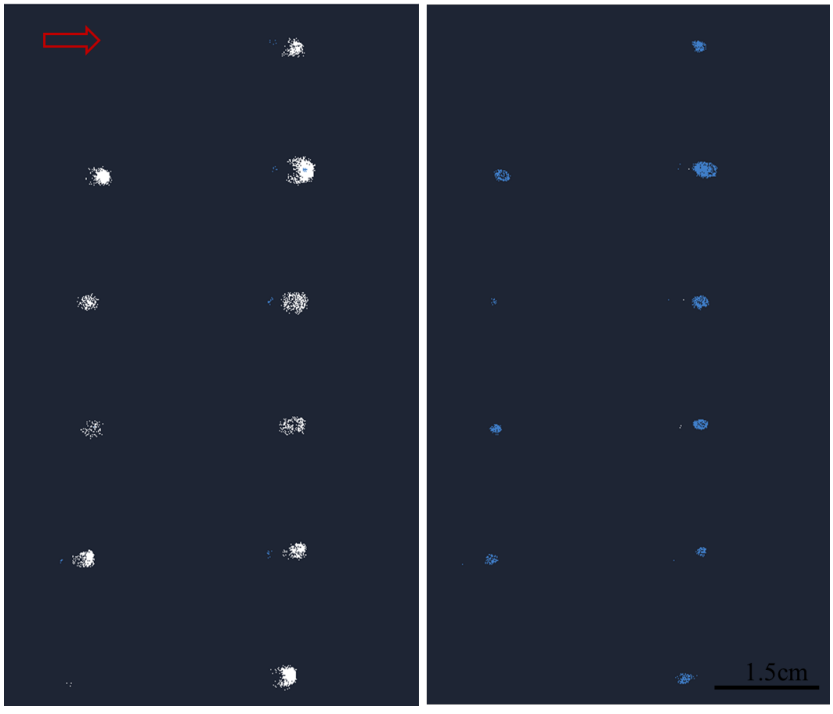

Figure 9. Two raw images of data as shown from the camera in Metavision, taken 0.2s apart, showing flow retardation.

The above figure, 9, shows that the EBC can successfully show changes in the flow velocity of

the pillars. All the pillars moving forward during increased flow velocity leave a white-marked positive event at the edge (left-hand image of figure 9). In comparison, when the pillars relax back to their equilibrium position after the air gust they leave a blue region of negative intensity change in the EBC image (right-hand side of 9. A complete colour change of the array indicates a shift in velocity speed. Here, in this figure, all the pillars changing from white to blue indicates that the flow over them is decelerating and the pillars are relaxing back to their equilibrium position, the opposite would be true for flow acceleration.

4.3. Cross flow disturbance

The results of the test in which the angle of the air gun relative to the centre row of pillars changed are as shown below in 10. This test mimics a change in freestream angle or crosswinds over the sensing wing. It can be seen that there is a rather constant phase difference of $\pi\mathrm{rad}$ in the motion between the rows of pillars (top and bottom rows nearly anti-phase). This indicates that the disturbance is moving at a constant speed along the span of the wing.

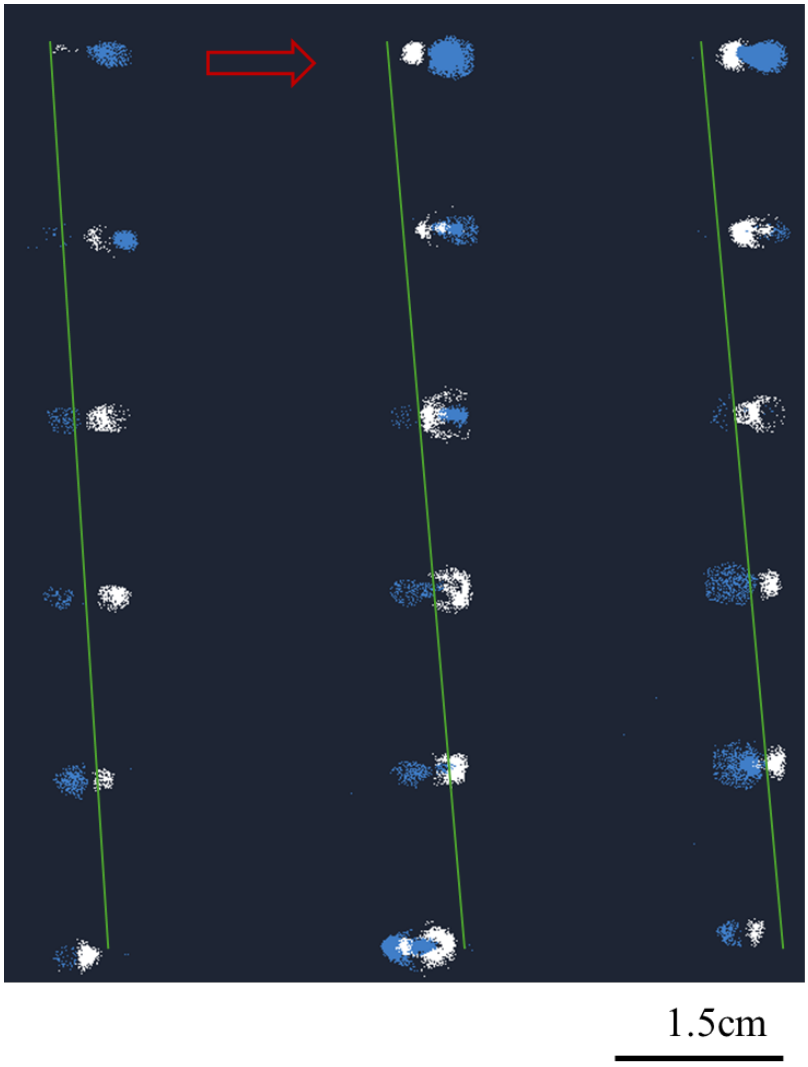

Figure 10. Raw image of data as shown from the camera in Metavision, with pillar phase difference in columns highlighted with green lines.

5. Conclusions

The results above demonstrate the feasibility of EBCs to be used to detect flow characteristics impacting a wing equipped with bio-inspired wind-hairs, over specific regions of interest, during specific gust conditions in both water and air. The results show potential for future fly-by-feel strategies where the EBCs can be used to monitor the flow patterns passing over the array of sensory hairs. Machine learning will help to train the system for specific events and to use the resulting workflow for monitoring or flow control.

The specific regions of interest are localised and centred around the pillar tips, which allows for sophisticated data collection and processing. Comparing EBCs to PIV, there is a lower event/s rate

< 1MEv/s, allowing for less data to be collected and easier, quicker processing. In addition, spatiotemporal information of the events along the pillar array makes it easier to distinguish coherent events from background noise, as we can expect a certain degree of consistency in the event patterns over the array. The results show that using the pillars with the EBC successfully distinguishes flow structures of the scale of the array.

The study has shown promise for future applications but is still in its infancy. The EBC requires a high-quality, powerful light source, which reduces the number of real-world applications. It is suggested that for future testing with the pillar and EBC setup, the tip marking of the pillars needs to improve to detect edge events better. A single reflective sphere attached to the pillar tips may help to give an improved localised pattern. Furthermore, one may use wave-guiding features of transparent silicone hairs or optical fibres as the sensing hairs, which could disregard the need for external illumination and provide a better quality of the tip spots.

The future applications for this study could include online flow monitoring via a machine learning algorithm that can detect the pattern of known flow structures over the pillars. This could allow for the implementation of flow control loops, which are designed to react to specific flow patterns.

6. Acknowledgements

The position of Professor Christoph Bruecker is co-funded as the BAE SYSTEMS Sir Richard Olver Chair and the Royal Academy of Engineering Chair (grant RCSRF1617/4/11) which is gratefully acknowledged. Thank you to City, University of London for part funding the PhD position of Alecsandra Court. We also thank the support from Dr. Chetan Yagadeesh for funding the camera. Finally, we also thank the Worshipful Company of Scientific Instrument Makers for the funding alongside the postgraduate award.

References

Court, A., & Bruecker, C. (2024). Fly by feel: Flow event detection via bioinspired wind-hairs. *Fluids*, *9*(3). Retrieved from `https://www.mdpi.com/2311-5521/9/3/74` doi: 10.3390/fluids9030074

Court, A., Selim, O., & Bruecker, C. (2023). Design and implementation of spanwise lift and gust control via arrays of bio-inspired individually actuated pneumatic flaplets. *International Journal of Numerical Methods for Heat and Fluid Flow*, *33*(4), 1528–1543.

Delbruck, T., & Lichtsteiner, P. (2007). Fast sensory motor control based on event-based hybrid neuromorphic-procedural system. In *2007 ieee international symposium on circuits and systems (iscas)* (p. 845-848). doi: 10.1109/ISCAS.2007.378038

Gallego, G., Delbrück, T., Orchard, G., Bartolozzi, C., Taba, B., Censi, A., ... Scaramuzza, D. (2022). Event-based vision: A survey. *IEEE Transactions on Pattern Analysis and Machine Intelligence*, *44*(1), 154-180. doi: 10.1109/TPAMI.2020.3008413

Lichtsteiner, P., Posch, C., & Delbruck, T. (2008). A 128$\times$ 128 120 db 15 μs latency asynchronous temporal contrast vision sensor. *IEEE Journal of Solid-State Circuits*, *43*(2), 566-576. doi: 10.1109/JSSC.2007.914337

Mahowald, M. (1992, August). *VLSI analogs of neuronal visual processing: a synthesis of form and function.* California Institute of Technology. doi: 10.7907/Z9CZ35CD

Mead, C. (1989). *Analog vlsi and neural systems*. USA: Addison-Wesley Longman Publishing Co., Inc.

Son, B., Suh, Y., Kim, S., Jung, H., Kim, J.-S., Shin, C., ... Ryu, H. (2017). 4.1 a 640×480 dynamic vision sensor with a 9µm pixel and 300meps address-event representation. In *2017 ieee international solid-state circuits conference (isscc)* (p. 66-67). doi: 10.1109/ISSCC.2017.7870263

Uruba, V., & Procházka, P. (2019, 11). The Reynolds number effect on dynamics of the wake behind a circular cylinder. *AIP Conference Proceedings*, *2189*(1), 020023. Retrieved from https://doi.org/10.1063/1.5138635 doi: 10.1063/1.5138635

Willert, C., & Klinner, J. (2023). Time-resolved velocity profile measurement using event-based imaging. In *15th international symposium on particle image velocimetry–ispiv 2023.*

Willert, C. E. (2023). Event-based imaging velocimetry using pulsed illumination. *Experiments in Fluids*, *64*(5), 98.